Journal of Physics and Chemistry of Solids 179 (2023) 111369

Contents lists available at ScienceDirect

Journal of Physics and Chemistry of Solids

journal homepage: www.elsevier.com/locate/jpcs

# Negative differential resistance effect and current rectification in $WS_2$ nanotubes: A density functional theory study

Mohammad Acef Ebrahimi [a], Somaieh Ahmadi [a,*], Abdus Salam Sepahi Molla [b], Santanu K. Maiti [c]

[a] Department of Physics, Imam Khomeini International University, Qazvin, Iran
[b] Department of Physics, Ferdowsi University Mashhad, Mashhad, Iran
[c] Physics and Applied Mathematics Unit, Indian Statistical Institute, 203 Barrackpore Trunk Road, Kolkata, 700 108, India

ARTICLE INFO

*Keywords:*
$WS_2$ nanotubes
Spin-orbit coupling
Negative differential resistances
Current rectification

ABSTRACT

Electronic properties of (n,0) zigzag tungsten disulfide $WS_2$ nanotubes and transport properties of (7,0) zigzag nanotube heterojunction are investigated by utilizing non-equilibrium Green's function formalism (NEGF). The results reveal that inclusion of the spin-orbit (SO) coupling significantly reduces the value of the band gap about 15.52\%. Additionally, strong negative differential resistances take place in voltage regions between −0.2 and −0.4 V as well as between −0.5 and −0.6 V. Moreover, temperature dependent transport properties are elaborately investigated in this work. The results show that, as the temperature increases to 600 K the stronger negative differential resistance occurs in both positive and negative bias voltages. Finally, a reasonably large degree of rectification ratio can be established. Our analysis can provide a comprehensive perspective on the NDR effect and current rectification in $WS_2$ nanotubes and can be used as a beneficial guide for future designing of novel logical and nanoelectronic and spintronic devices.

## 1. Introduction

Following the discovery of graphene, considerable interests in experimental and theoretical researches have been concentrated on nano-scale two-dimensional (2D) electronics. Extremely high carrier mobility of graphene makes it a very good candidate for building fast field effect transistors [1–5] and many more. However, pristine graphene has no band gap which is a serious important flaw for applications of logic transistors to achieve the suitable on/off ratio [2,6]. Significant theoretical and experimental efforts, such as chemical decorations [7–10], cutting of graphene into nanoribbons [11–13] and bond cleavage by impurity doping [14–17], have been used to open a proper band gap in graphene. These techniques reduce the mobility of carriers. Therefore, some researches proposed utilizing graphene-like semiconductor materials like Transition Metal Dichalcogenides (TMDs) which can exhibit metallic, semiconducting, and superconducting phases [18–22].

Multilayer and monolayer structures, nanotubes and nanoribbons of TMDs have been synthesized and studied in large quantities [23–27]. Due to the unique structural and electronic properties, including high mobility [28,29], organic-like flexibility [30], and larger on/off ratio [31], TMDs have been considered as promising candidates for the field-effect transistors (FETs). Tremendous experimental and theoretical attempts to study the electronic transport properties of layered and nanotube structures of TMDs have been done [32–39].

Understanding the novel properties of the one-dimensional transition metal dichalcogenides is highly significant for the development of high performance nanoelectronic devices and advancing related technologies. Tungsten Disulfide Nanotubes ($WS_2$NTs) are one-dimensional nanostructures similar to $MoS_2$ and $WSe_2$ nanotubes in terms of crystal lattice type and lattice parameters [40,41]. $WS_2$ nanotubes have been synthesized in different diameter sizes, from diameters of 3 and 5 nm–100 nm and also lengths of several micrometers [42–45] and their transport properties have been experimentally studied in field effect transistors [36]. Theoretical studies on band structure of $WS_2$ nanotubes show that zigzag and armchair nanotubes have direct and indirect band gaps, respectively, with the values which get enhanced by increasing the diameters of the tubes [46,47]. Ghorbani-asl et al. studied electro-mechanical properties of $WS_2$ nanotubes [48]. Field emission characteristics of multi-walled $WS_2$ nanotubes under axial strain have

* Corresponding author.
*E-mail address:* s.ahmadi@sci.ikiu.ac.ir (S. Ahmadi).

https://doi.org/10.1016/j.jpcs.2023.111369
Received 1 February 2023; Received in revised form 3 April 2023; Accepted 9 April 2023
Available online 27 April 2023

been experimentally investigated by Grillo et al. [49]. Additionally, $WS_2$, like other families of dichalcogenides, is a combination of heavy atoms which led to much larger SO coupling compared to carbon atoms. This feature promises to generate, detect and manipulate spin currents which triggered tremendous interest to investigation of SO effect on electronic structures and transport characteristics of $WS_2$.

In the present study, a comprehensive analysis on electronic band structure and transport properties of $WS_2$NTs are carried out by employing Non-Equilibrium Green Function (NEGF) method combined with first principal density functional theory (DFT). Electronic structure of single wall zigzag $WS_2$ nanotubes with various diameters is studied. Transport properties through the single-wall $WS_2$ nanotube hetero-junctions for proper diameter with and without SO coupling are investigated. Our results show that the SO coupling decreases the band gap which has the remarkable effects on transport properties. Although the NDR occurs in the absence of SO coupling, the presence of SO coupling amplifies intensity of NDR. Moreover, increment of temperature affects the electronic structure and current-bias characteristics even in the absence of SO coupling, which can yield giant NDR. It is worthy to note that involving the SO coupling in first principal calculations doubles the matrix size of Green's function and hence in the self-consistent loop the converge rate slows down considerably. The best of our knowledge, due to huge computational burden, many theoretical investigations on electronic transport in the framework of first-principles calculation for nanodevices neglect the SO coupling. The main aim of this study is to include the SO coupling in the First-principles calculation for electronic band structure and transport properties of $WS_2$ nanotubes.

## 2. Methods and computational details

In this study First-principles calculations have been performed to study the electronic band structure and electronic transport properties of $WS_2$NTs using density functional theory in conjunction with NEGF method by the Landauer-Buttiker approach implemented by OpenMX package [50]. The sampling of the Monkhorst-Pack grids [51] in the first Brillouin Zone was assumed to be $1 \times 1 \times 60$ for calculations of the structural relaxations, electronic band structure, and quantum transport characteristics. The kinetic energy cut-off was set to 300 Ry and the convergence criterion for energy was set to$10^{-7}$ Ry. The self-consistent solution of the Cohn-Sham equations was continued until the force on the atom exceeded at least $10^{-5}$ Ry/Å. The structure relaxation was carried out by utilizing the Broyden-Fletcher-Goldfarb-Shanno (BFGS), the rational function method (RF), and the direct inversion iterative sub-space (DIIS) method as implemented in the OpenMX package [52–57]. The calculations in this study were performed using the Pardew Wang exchange-correlation function under the local spin density approximation (LSDA-PW) [58]. Additionally, pseudo-atomic orbitals (PAO) which applied by S7.0-s2p2d1f1 and W7.0-s3p2d2f1, were considered as basis wave functions.

Based on NEGF method the electronic transport calculations have been carried out using OpenMX package. In this formalism, the finite-bias transmission coefficients have been invoked as follows

$$T(\varepsilon, V) = tr(\Gamma_L G_C \Gamma_R G_C), \tag{1}$$

where tr indicates trace of matrix and $\Gamma_{L(R)}(\varepsilon, V) = \mathrm{Im}(\Sigma_{L(R)}(\varepsilon, V) - \Sigma^{+}_{L(R)}(\varepsilon, V))$ is the broadening matrices of left (right) lead [59]. $G_C$ represents the Green's function of scattering region. Using Landauer-Buttiker formula, the current is calculated by

$$I = e \Big/ h \int_{-\infty}^{+\infty} T(\varepsilon, V)[f_L(\mu_L, T) - f_R(\mu_R, T)]d\varepsilon. \tag{2}$$

here, e and $h$ are the electron charge and the Planck's constant, respectively. $\mu_{L(R)} = \mu \pm \frac{|e|V}{2}$ is the chemical potential of left (right) leads, $T$ is the equilibrium temperature, $V$ is the bias voltage which is applied between the source (left lead) and drain (right lead), and $f_{L(R)}(\varepsilon, \mu_{L(R)})$ is the Fermi-Dirac distribution of left (right) lead at equilibrium.

In DFT calculations, any change in the form of potential is added to the Kohn-Sham Hamiltonian of the system, and self-consistent calculations are used to extract physical properties. Therefore, the spin-orbit interaction is also added to the Hamiltonian and the calculations are performed in its presence. In Kohn-Sham Hamiltonian scheme, the spin-orbit potential ($V_{SO}$) is expressed by

$$V_{SO} = \sum_{l,m} V_l^{SO} \vec{L} . \vec{S} |l, m\rangle\langle l, m|,$$

where $\vec{L}$ and $\vec{S}$ are angular momentum and spin operators, respectively. $|l, m\rangle$ indicates the angular momentum states. $V_l^{SO}$ is strength of spin-orbit coupling for each state. In the other calculation method, first-principles calculations are combined with a tight-binding Hamiltonian model for investigation of spin dependent properties [60,61].

Changes in temperature also lead to changes in the Fermi-Dirac distribution function of each lead in the Landauer equation.

## 3. Results and discussion

The stable structure of orthorhombic primitive unit cell of $WS_2$NTs is shown in Fig. 1. The optimized lattice parameters and the bandgaps of $WS_2$NTs primitive unit cell are listed in Table 1.

To elucidate the dependence of band gap on tube diameter, the electronic band structure along high symmetry directions of the first Brillouin zone has been calculated. We have examined the zigzag tubes of different diameters (n = 7, 10, 14, 18, and 22), as shown in Fig. 2. The conduction band minimum (CBM) is exactly above the valence band maximum (VBM) at the gamma point which exhibits a direct band gap in zigzag nanotubes. The results of calculations show that the band gap increases with rising the nanotube diameter, which is in consistent with literature [47]. Note that the increasing tendency of the band gap with increasing nanotube diameter stems from the weakening quantum confinement. Therefore, nanotubes with bigger diameter are not suitable for electrical transport phenomena, and hence, we have performed quantum transport calculations on (7,0) nanotube.

Fig. 3 shows a device consisting of homo-junctions of the (7, 0) zigzag nanotube primitive unit cell. The device is composed of two parts; scattering region (C) and semi-infinite left and right electrodes (L, R) where all of them are made of (7, 0) zigzag nanotube. A high bias voltage is applied to left electrode in all calculations.

The zero bias transmission coefficient of (7,0) zigzag nanotube without SO coupling is displayed in Fig. 4b, which is consistent with the computed band structure of scattering/electrode region primitive unit cell as shown in Fig. 4a. Fig. 4a shows the calculated band structure

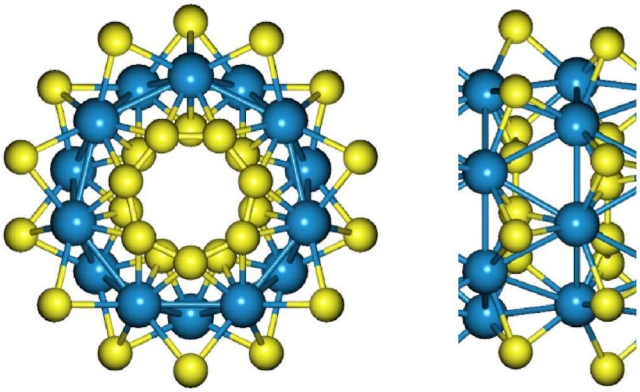

**Fig. 1.** (Color online). Schematic diagram of (7,0) zigzag $WS_2$ nanotube primitive cell.

**Table 1**
Relaxed lattice constant (a, b) and band gap (Eg) of five primitive unit cell of (n,0) zigzag $WS_2$NTs.

| Nanotubes | a (Å) | b (Å) | $E_g$ (meV) |
|---|---|---|---|
| (7,0) | 25.23 | 25.23 | 170 |
| (10,0) | 31.53 | 31.53 | 400 |
| (14,0) | 44.15 | 44.15 | 862 |
| (18,0) | 56.76 | 56.76 | 1243 |
| (22,0) | 69.37 | 69.37 | 1504 |

without SO coupling along the Γ-X high symmetry directions of the first Brillouin zone. The band structure is calculated by PBE methods which is in agreement with the computational methods in Ref. [62]. The direct band gap is about 0.18 eV where there is no transmission coefficient. The transmission coefficient for region of energy $\varepsilon > 0$ is higher than that of energy region $\varepsilon < 0$ for (7, 0) $WS_2$ heterojunction. This behavior of transmission coefficient arises from lower hole mobility than that of electron mobility. In addition, the band structure exhibits that the number of eigenstates for electron is more than that of hole, which reflects the high values of the transmission coefficients for electrons.

To have a better understanding of the dependence of transmission coefficient on bias voltage, the transmission coefficient versus the electron energy for different biases is depicted in Fig. 5. The results show that by increasing the bias voltage, the values of the transmission coefficients change near the transmission gap. In fact, the transmission curves shift to the right by increasing the value of bias voltage and the size of the transmission gap increases at high voltages. As shown in Fig. 5a, when the positive bias is applied, the chemical potential of the left electrode increases and the potential of the right electrode decreases. Therefore, the right electrode band gap shifts to the right, away from the Fermi energy. As a result, the transmission coefficient gradually shifts to the right, and the left edges of areas where the transmission coefficients are zero become closer to Fermi energy. Therefore, the total transmission coefficient in the bias window gradually leads to the current enhancement. However, when a negative bias is applied to the system, the chemical potential of the left electrode decreases and the chemical potential for the right electrode increases. Therefore, the transmission coefficients shift to the left. The left edges of areas with zero transmission coefficients move away from Fermi energy, as shown in Fig. 5b. At positive voltages changes in transmission coefficients are imperceptible in the bias window with voltages between 0.2 and 0.4 V which leads to weak electrical current. Our results reveal that the shapes and positions of the transmission coefficients are affected by bias voltages. In fact, this effect arises from the dependence of electrical transport on the electronic band structure of the electrodes and scattering regions. By overlapping.

of similar bands in the bias window of the left (right) electrodes, the electron transmission channel will be opened, as reported earlier [63].

Now we study the effect of SO coupling on band structure and transmission coefficient. As shown in Fig. 6a, the energy band gap in the presence of SO coupling gets decreased compared to what we obtained for the SO coupling free case. In fact, the band gap decreases from 0.174 to 0.147 eV, which shows a reduction of about 15.52\%. Moreover, as it is shown in the figure the eigenstates in the band structure are doubled in the presence of SO coupling. The zero bias transmission coefficient increases significantly for both the highest occupied molecular orbital (HOMO) and the lowest unoccupied molecular orbital (LUMO) in the

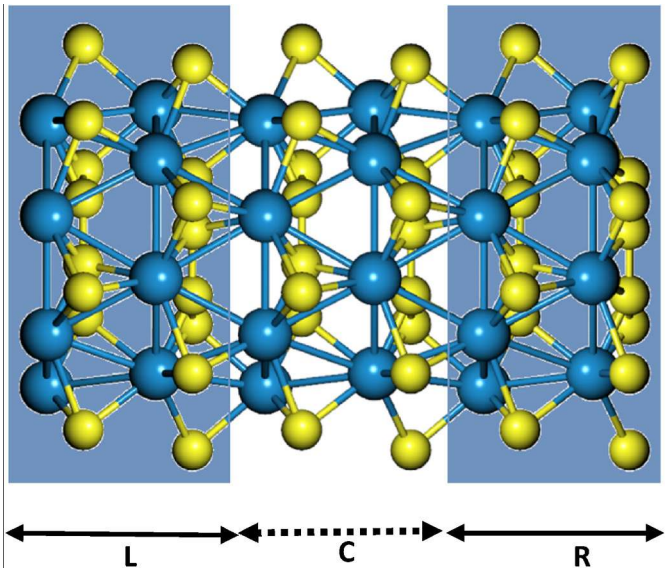


**Fig. 3.** A device composed of the homo-junctions of electrodes to a channel. The blue background identifies the electrodes, which from left to right are the left electrode (source), channel (scattering region), and right electrode (drain), respectively.

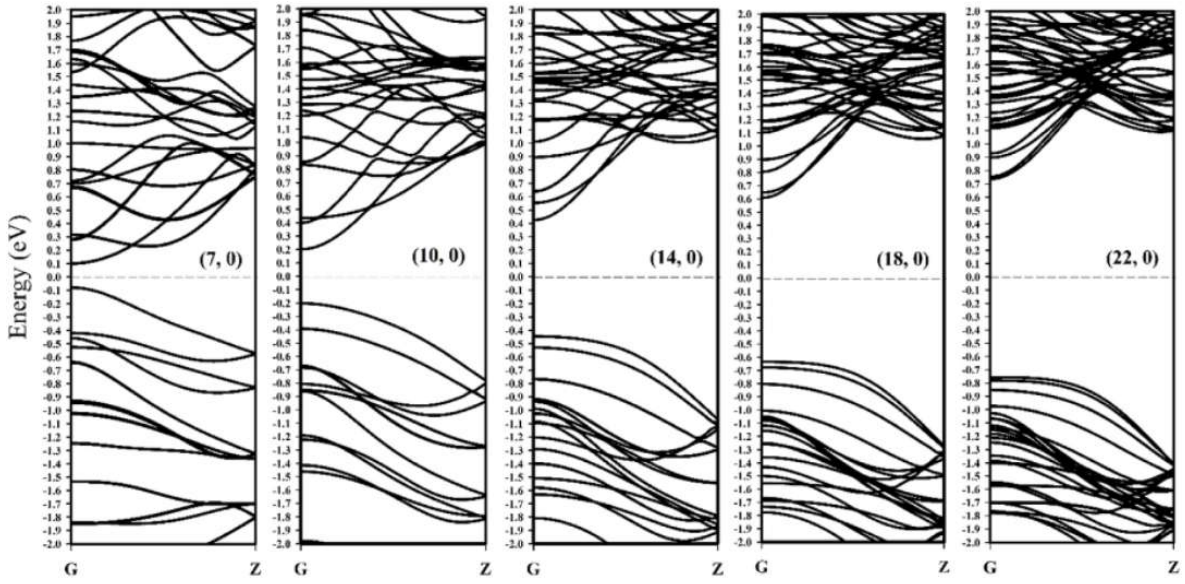


**Fig. 2.** The band structure of (n, 0) zigzag tungsten disulfide $WS_2$ nanotubes for n = 7, 10, 14, 18, and 22.

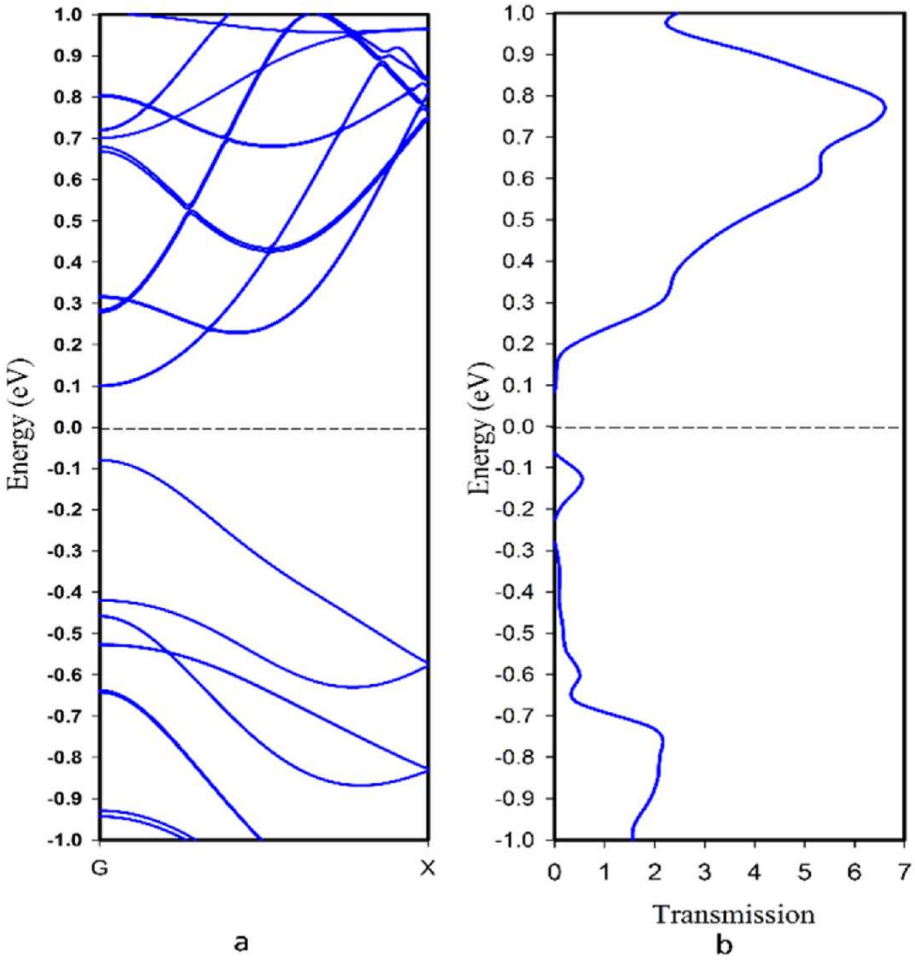


**Fig. 4.** (Color online). a) The band structure of (7,0) zigzag nanotubes and b) the transmission coefficient as function of energy at zero bias.

presence of SO coupling as shown in Fig. 6b. Furthermore, in the presence of SO coupling the transmission gap reduces, which is consistent with reduction of band gap in electronic band structure.

For better realization of the effect of temperature on current, we have studied the transport characteristics at some typical temperatures (200 K, 300 K, 400 K and 600 K). Fig. 7 shows the current-voltage characteristic at 200 K, 300 K, 400 K and 600 K. As shown in Fig. 7b, the current versus the bias voltages is approximately equal at T = 200 K and T = 300 K. In addition, a weak NDR behavior is observed at bias voltage range of - 0.6 to −0.7 V and bias voltage range of 0.7–0.8 V at 300 K. At bias voltage range of 0.1–0.2 V and −0.2 t0 -0.4 the NDR behavior take places at 400 K. Compared to 200 K, 300 K and 400 K, the current-voltage curve shows remarkable changes at 600 K. At the bias voltage range of 0–0.1 V, the current increases sharply, and also at the bias voltages between 0.1 and 0.3 V, it shows a sharp decrease which corresponds to a strong NDR effect. There is also another week NDR effect in bias voltage range of 0.7–0.8 V. Interestingly, a strong NDR behavior takes place in negative bias voltage between −0.6 and −0.4 V. Therefore, the intensity of NDR increases with the rise of temperature. Moreover, at 600 K, the current is higher than that of the other temperatures. In fact, by increasing temperature, more electrons.

obtain adequate energy to pass the band gap. These electrons participate in conductance and may lead to an enhancement in the current. As it can be determined from the results, the NDR behavior of the system depends on the value of the bias voltage as well as the temperature of the system. Moreover, our results show that a remarkable variation in current occurs at bias voltage range of −1 to 1 V independent of temperature. Therefore, all calculations will be done in this voltage range. Furthermore, the electron-phonon coupling is common concept for designing of electronic devices even room temperature. Zhang et al. showed experimentally reduction of thermal conductivity by increasing the temperature for $WS_2$ sheets [64]. Thermal conductivity in two-dimensional materials decreases due to phonon scattering at boundaries and quantum confinement effect [65,66]. Therefore, we except that the thermal conductivity of $WS_2$ tubes decrease with increasing temperature duo to scattering at boundaries and quantum confinement effect in nanotubes.

Fig. 8, shows the band structure of (7,0) zigzag $WS_2$ nanotube without SO coupling at zero bias voltage. Fig. 8a shows that the valence band is very close to the Fermi energy and the conduction band moves away from the Fermi energy. At 600 K, the valence and conduction bands move slightly compared to the positions of these bands at room temperature. Similar changes are also seen in the transmission coefficients. In addition, there is not a significant difference between zero bias transmission coefficients at.

200 K, 300 K and 600 K. Therefore, the current for zero voltage is the same at all temperatures as seen in Fig. 7.

In order to study the SO effect on current, the electrical current as a function of bias voltage in the absence of SO and in the present of SO at 300 K is shown in Fig. 9. In the absence of SO, the current is slightly asymmetric at positive and negative biases, but in general, the current increases with increasing the bias (both positive and negative). Our findings show that the maximum value of the current is about a few tenths of Micro Ampere which is in agreement with the experimental results [36]. In addition, a negative differential resistance (NDR) can be observed in the positive bias voltage. As it is clearly shown in the figure

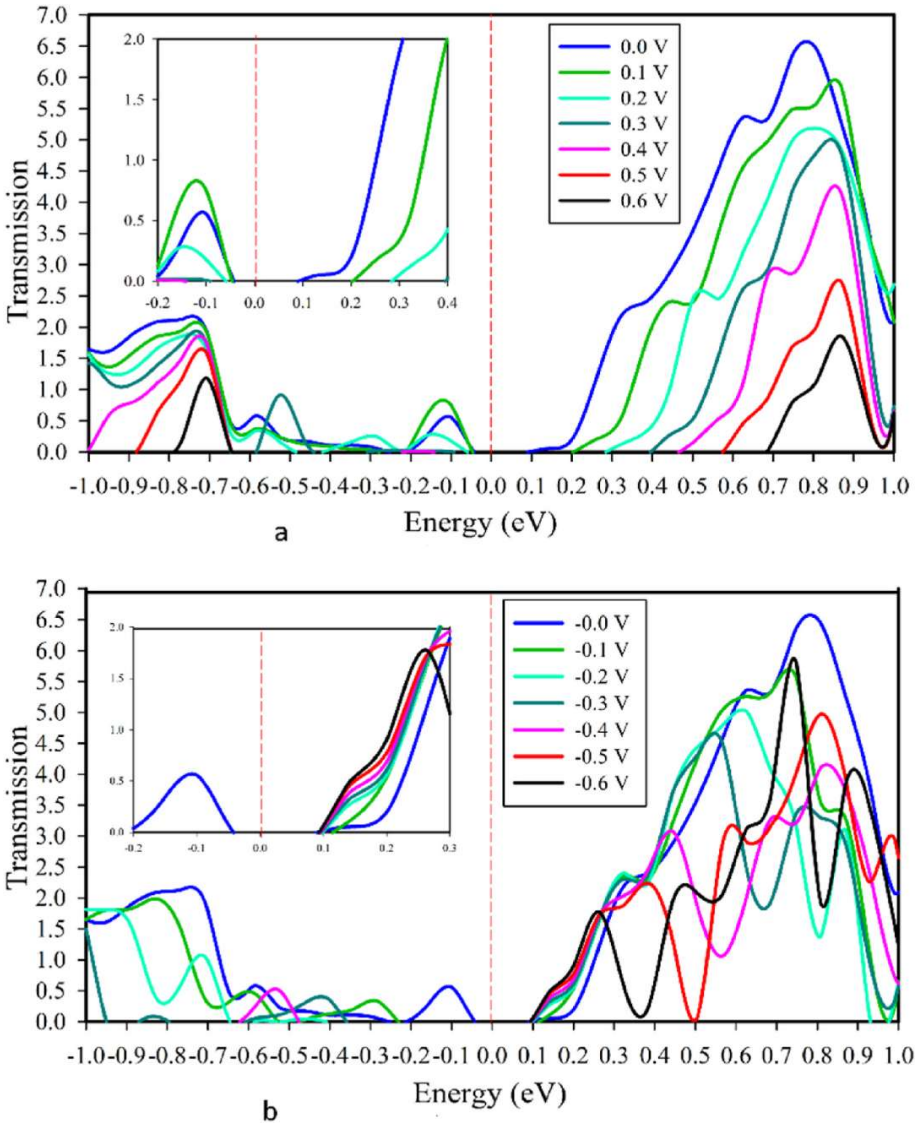


**Fig. 5.** (Color online). Transmission coefficients of (7,0) zigzag nanotubes as a function of energy for (a) positive biases and (b) negative biases.

the electrical current increases with increasing bias voltage between 0 and 0.7 V, then it decreases for the higher voltages. Increasing the bias voltage at the terminals of some electrical devices in some circumstances leads to a decrease in electrical current known as NDR behavior which is the case here for bias voltages in the range of 0.7–0.8 V. In fact, when bias voltage is applied on the system, a mismatch occurs between the electronic band structures of the electrodes and the scattering region. Therefore, the electrons are not able to find some suitable states to tunnel across the structure from the left to the right electrode which can lead to the NDR behavior of the system. This feature looks interesting when it is compared to a typical resistor in which due to the Ohmic law, the applied voltage increases the current proportionally, resulting in a positive resistance. As a matter of fact, a negative resistance produces power.

which can increase and amplify electrical signals under some particular conditions. Therefore, NDR effect, which is occurred in (7,0) zigzag nanotubes, will strengthen the applications of these nanotubes as electronic devices. As expected, the electrical current changes in the present of SO coupling effect as demonstrated in Fig. 9. In positive bias voltages, the current enhances by increasing the bias voltage. As shown in Fig. 9, when negative bias voltages are applied to the system, in some specific voltages the electrical current reduces by increasing the bias voltage. So, at bias voltage between −0.1 and −0.2, and also between −0.4 and −0.5 V, strong NDR behavior is observed. This could play an interesting role in the process of controlling the electronic and transport properties of $WS_2$ zigzag nanotubes and offering them as practical logic devices. The NDR effect is caused by band structure changes, so it can be seen asymmetrically in forward or negative (positive) bias. For example, Kim et al., showed the asymmetric NDR in graphene heterostructures which can be converted to symmetric NDR by adding the defect [67]. Additionally, as reported in reference 32, an asymmetric NDR addressed for $WSe_2$ by Yu et al.

Now, we focus on different aspects of the physical system. In Fig. 10, we show the dependence of the band gap on bias voltage (V). The results are shown in the absence (blue curve) and presence (red curve) spin-orbit coupling, for the two bias polarities. Here the temperature is fixed at 300 K. The key feature is that, we can have a large variation in band gap as a function of the voltage bias, and it becomes more pronounced when the system is free from spin-orbit coupling. Moreover, the changes are also different in the two bias polarities. In fact, negative/positive bias voltage shifts the energy band of left and right leads, which leads to suppression of electron transmission in scattering channel. Therefore, the region in which the electron transmission does not occur depends on the bias voltage, as shown in Fig. 5.

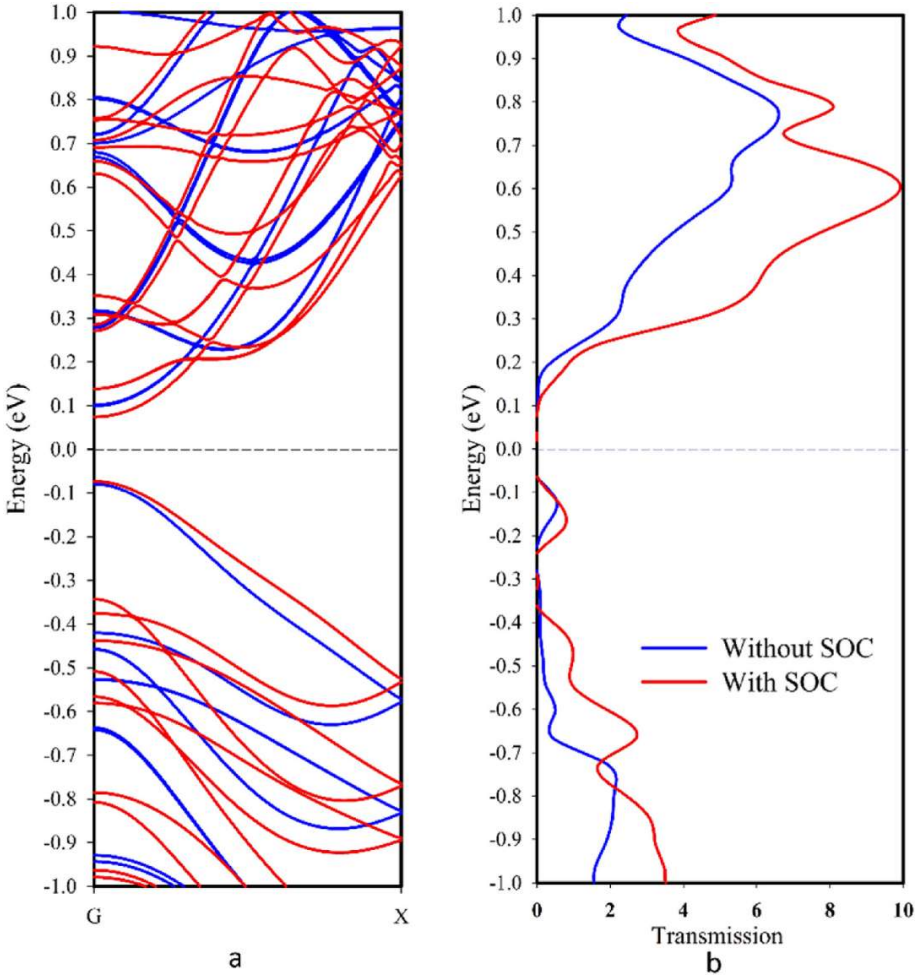


**Fig. 6.** (Color online). (a) Band structure of a (7,0) zigzag nanotube without SO coupling (blue) and with SO coupling (red). (b) Zero bias transmission coefficients as a function of energy without SO coupling (blue) and with SO coupling (red).

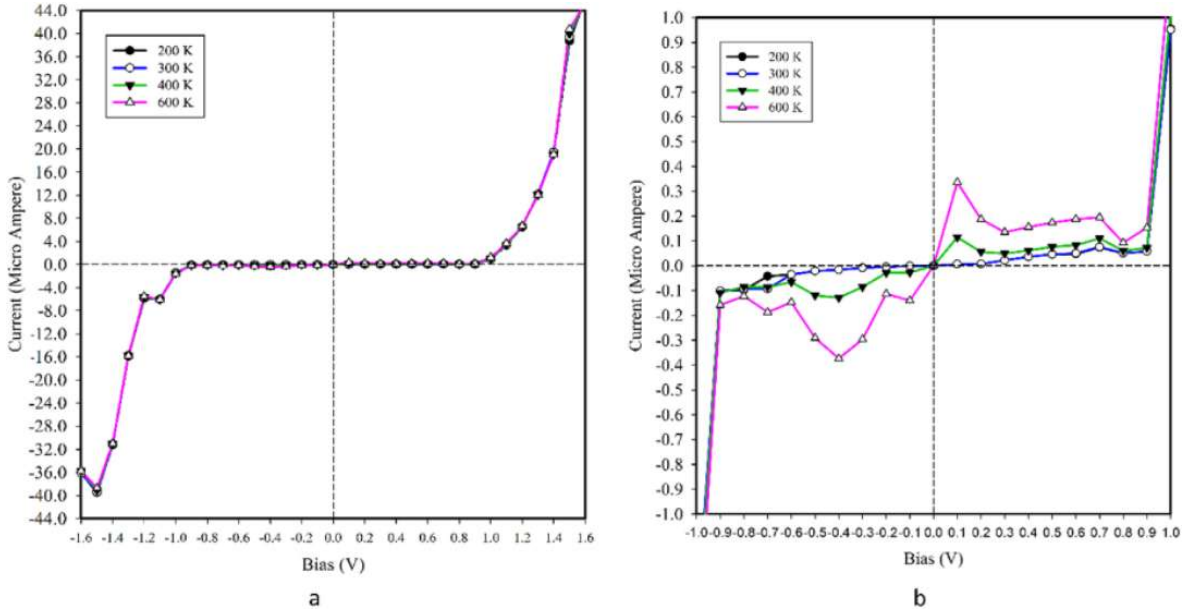


**Fig. 7.** (Color online). Current-voltage characteristics at 200 K, 300 K, 400 K and 600 K.

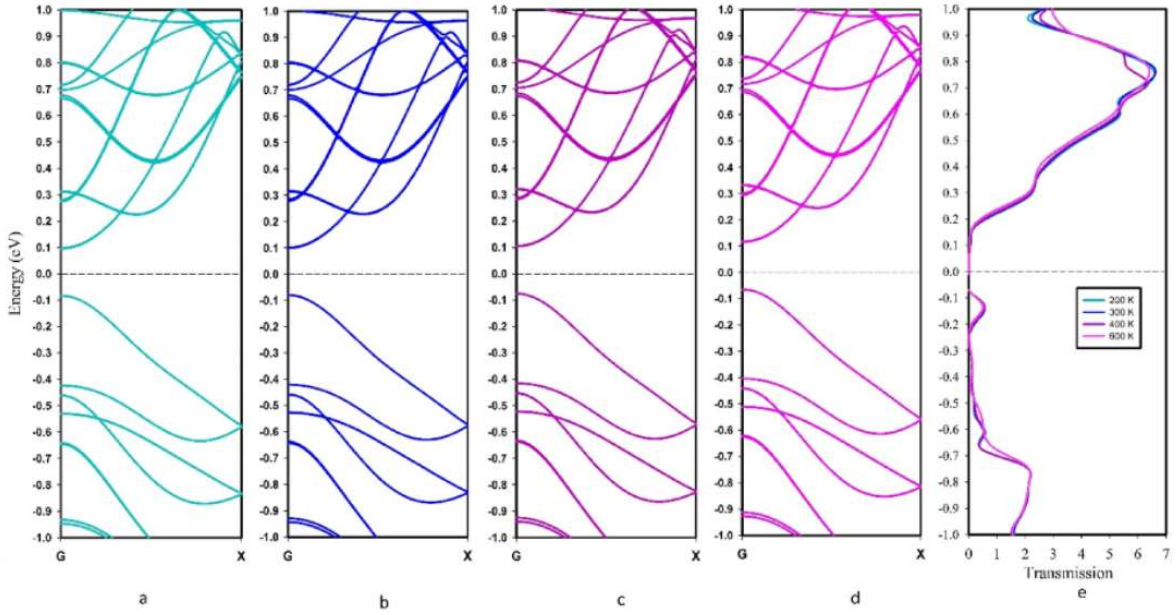


**Fig. 8.** (Color online). Zero bias band structure at (a) 200 K, (b) 300 K, (c) 400 K, (d) 600 K, and (e) the transmission coefficient as function of energy.

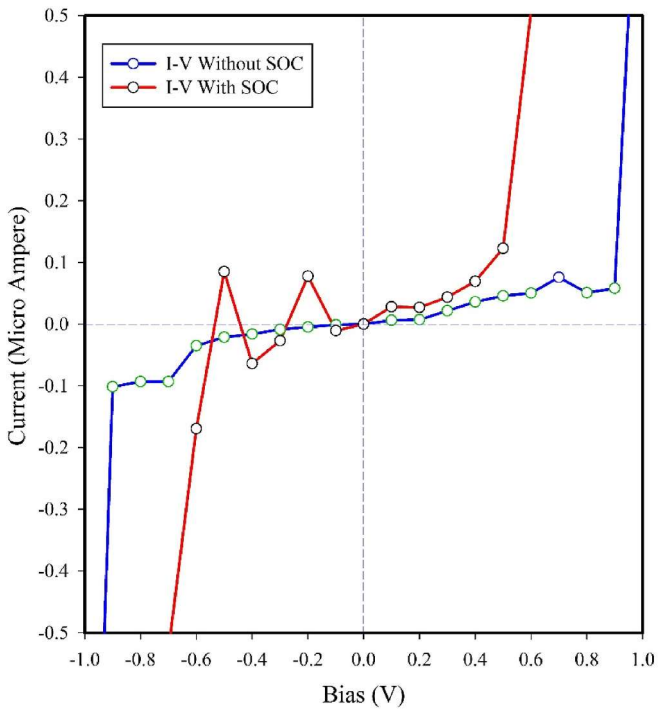


**Fig. 9.** (Color online). Current as a function of bias voltage in the absence (blue) and presence (red) of the SO coupling at 300 K.

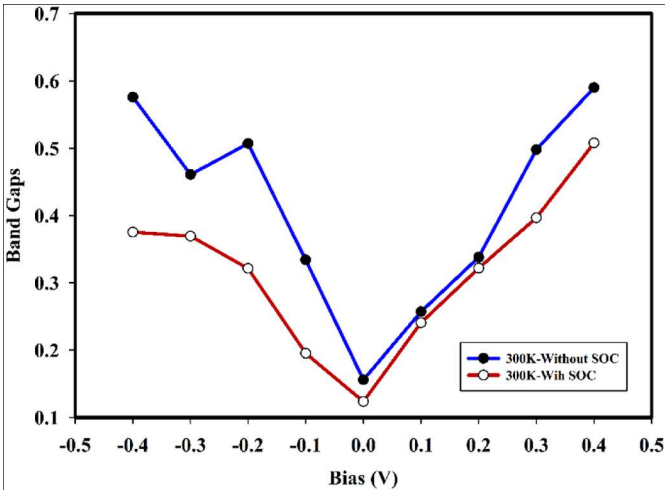


**Fig. 10.** (Color online). Band gap as function of voltage at 300 K with SO coupling and without SO coupling.

At this stage it is indeed important to check, how the energy band gap of the system varies with the temperature. The results are illustrated in Fig. 11. From Fig. 10 it has already been established that, more variation is expected for the spin-orbit field free case, and accordingly, in Fig. 11 the results are worked out in the absence of SO coupling. Three different temperatures are considered, and the corresponding variations are described by three different colored curves. Like Fig. 10 here also we consider both the positive and negative bias polarities. The results are very interesting and important as well. Both for the two bias polarities, the energy band gap changes with temperature. The variation of this gap is quite less sensitive (like what is seen in Fig. 10 for the positive bias than its counterpart. The variation of energy band gap with system temperature leads to the possibilities of designing charge and spin based electronic devices. The threshold voltage for non-zero current can be tuned selectively by regulating the system temperature.

Finally, we discuss another interesting physical phenomenon that is exhibited by the nanotube. This is the charge current rectification [68, 69]. The use of rectifiers is almost everywhere in electronic circuits. So, if we can get the rectification operation, then it will be another key advantage of our physical system. Now, to have the current rectification, the primary requirement is that the currents should be different in two bias polarities. There are different prescriptions to make these two currents different. The simplest one is the existence of disorder in the system, or it can be substantiated by means of different couplings of the system with the contact leads. For our system, we see that a reasonably large degree of current rectification (~60%) can be obtained even at too low bias voltage (see Fig. 12). That is indeed a very good sign. As we get much favorable response for the spin-orbit field free case, which we confirm through our exhaustive numerical calculations, in Fig. 12 we show the results only for the field free case. The degree of rectification

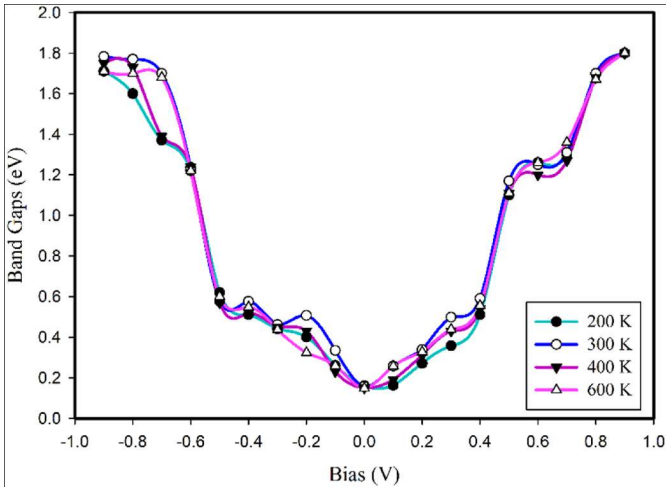


**Fig. 11.** (Color online). Band gap as function of voltage at 200 K, 300 K, 400 K and 600 K whitout SO coupling.

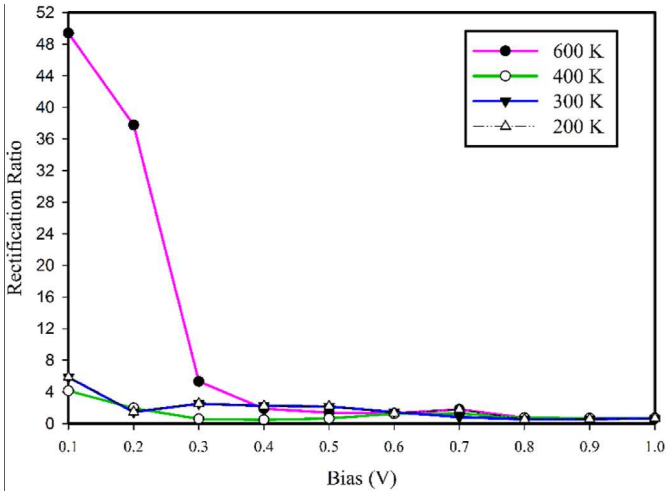


**Fig. 12.** (Color online). Rectification ratio as function of voltage at 200 K, 300 K, 400 K and 600 K whitout SO coupling.

decreases with increasing the bias voltage as well as the system temperature. So, we need to restrict ourselves within the low bias limit and low temperature region, to have a favorable response.

## 4. Conclusion

All the calculations related to electronic structural and transport properties have been performed by simulation method in the form of density functional theory and non-equilibrium Green's function approach, in which OpenMX computational code has been used. To ensure the accuracy of our computational and simulation work, we first calculated the electronic structural properties of (n,0) zigzag $WS_2$ nanotubes. Declining the diameter of nanotubes led to band gap reduction which is more suitable for investigation of SO coupling effect and transport properties. Our calculations show that the band gap decreases about 15.52\% in the presence of spin-orbit coupling. In addition, the transmission coefficient and current-voltage characteristics get significantly enhanced in presence of the SO coupling. Moreover, the results showed that stronger NDR effect occurs with SO coupling than that of without SO coupling. Furthermore, the strength of NDR extremely increases in both the negative and positive bias voltages with increasing the temperature, even in the absence of SO coupling. At the end, we have explored the phenomenon of current rectification. It has been observed that a reasonably large degree of current rectification can be substantiated at the low temperature and low bias region.

## Credit author statement

**Mohammad Acef Ebrahimi**: Data Curation, Formal analysis, Validation, Software, Conceptualization. **Somaieh Ahmadi**: Writing - Original Draft, Visualization, Project administration, Supervision, Data Curation, Resources, Formal analysis, Validation, Software. **Abdus Salam Sepahi Molla**: Visualization, Validation, Software, Editing. **Santanu K. Maiti**: conceived the study, wrote, reviewed, and edited the manuscript.

## Declaration of competing interest

The authors declare that they have no known competing financial interests or personal relationships that could have appeared to influence the work reported in this paper.

## Data availability

Data will be made available on request.

## References

[1] D.C. Elias, R.V. Gorbachev, A.S. Mayorov, S.V. Morozov, A.A. Zhukov, P. Blake, L. A. Ponomarenko, I.V. Grigorieva, K.S. Novoselov, F. Guinea, A.K. Geim, Nat. Phys. 7 (2011) 701–704.
[2] L. Liao, J. Bai, Y. Qu, Y.-C. Linb, Y. Lib, Y. Huan, X. Duan, Natl. Acad. Sci. 107 (2010) 6711–6715.
[3] Y.-M. Lin, K.A. Jenkins, A. Valdes-Garcia, J.P. Small, D.B. Farmer, P. Avouris, Nano Lett. 9 (2009) 422–426.
[4] A.S. Mayorov, R.V. Gorbachev, S.V. Morozov, L. Britnell, R. Jalil, L. A. Ponomarenko, P. Blake, K.S. Novoselov, K. Watanabe, T. Taniguchi, A.K. Geim, Nano Lett. 11 (2011) 2396–2399.
[5] Y.-M. Lin, C. Dimitrakopoulos, K.A. Jenkins, D.B. Farmer, H.-Y. Chiu, A. Grill, P. H. Avouris, Science 327 (2010), 662 LP – 662.
[6] X. Li, W.W. Cai, J.H. An, S.Y. Kim, J. Nah, D.X. Yang, R. Piner, A. Velamakanni, I. Jung, E. Tutuc, S.K. Banerjee, L. Colombo, R.S. Ruoff, Science 324 (2009) 1312–1314.
[7] L. Gan, J. Zhou, F. Ke, H. Gu, D.N. Li, Z.H. Hu, Q. Sun, X.F. Guo, NPG Asia Mater. 4 (2012) e31–e37.
[8] R. Balog, B. Jorgensen, L. Nilsson, M. Andersen, E. Rienks, M. Bianchi, M. Fanetti, E. Lagsgaard, A. Baraldi, S. Lizzit, Z. Sljivancanin, F. Besenbacher, B. Hammer, T. G. Pedersen, P. Hofmann, L. Hornekar, Nat. Mater. 9 (2010) 315–319.
[9] J.C. Dong, H. Li, J. Phys. Chem. C 116 (2012) 17259–17267.
[10] W.J. Zhang, C.T. Lin, K.K. Liu, T. Tite, C.Y. Su, C.H. Chang, Y.H. Lee, C.W. Chu, K. H. Wei, J.L. Kuo, L.J. Li, ACS Nano 5 (2011) 7517–7524.
[11] J. Hicks, A. Tejeda, A. Taleb-Ibrahimi, M.S. Nevius, F. Wang, K. Shepperd, J. Palmer, F. Bertran, P. Le Fevre, J. Kunc, W.A. de Heer, C. Berger, E.H. Conrad, Nat. Phys. 9 (2013) 49–54.
[12] X. Li, X. Wang, L. Zhang, S. Lee, H. Dai, Science 319 (2008), 1229–LP-1232.
[13] Y.W. Son, M.L. Cohen, S.G. Louie, Phys. Rev. Lett. 97 (2006), 216803-1–216803-4.
[14] N.R. Abdullah, H.O. Rashid, M.T. Kareem, C.-S. Tang, A. Manolescu, V. Gudmundsson, Phys. Lett. 384 (2020), 126350-126351-126350-8.
[15] H. Guo, R. Zhang, H. Li, X. Wang, H. Lu, K. Qian, G. Li, L. Huang, X. Lin, Y.-Y. Zhang, H. Ding, S. Du, S.T. Pantelides, H.-J. Gao, Nano Lett. 20 (2020) 2674–2680.
[16] L. Chen, F. Ouyang, S. Ma, T.-F. Fang, A.-M. Guo, Q.-F. Sun, Phys. Rev. B 101 (2020), 115417-1-115417-10.
[17] M. Tayyab, A. Hussain, Q. ul A. Asif, W. Adil, Comput. Condens. Matter 23 (2020) e00469-1-e00469-12.
[18] V. Bagga, D. Kaur, Mater. Today Proc. 28 (2020) 1938–1942.
[19] X. Hu, E. Xu, S. Xiang, Z. Chen, X. Zhou, N. Wang, H. Guo, L. Ruan, Y. Hu, C. Li, D. Liang, Y. Jiang, G. Li, CrystEngComm 22 (2020) 5710–5715.
[20] S. Kezilebieke, M.N. Huda, P. Dreher, I. Manninen, Y. Zhou, J. Sainio, R. Mansell, M.M. Ugeda, S. Dijken, H.-P. Komsa, P. Liljeroth, Commun. Phys. 3 (2020), 116-1-116-8.
[21] S.A. Tawfik, O. Isayev, C. Stampfl, J. Shapter, D.A. Winkler, M.J. Ford, Adv. Theory Simul. 2 (2019), 1800128-1-1800128-11.
[22] Z. Golsanamlou, L. Sementa, T. Cusati, G. Iannaccone, A. Fortunelli, Adv. Theory Simul. 3 (2020), 2000164-1-2000164-8.
[23] C. Sun, G. Zhang, Y. Shang, Z. Yang, X.J. Sun, Phys. Chem. Chem. Phys. 18 (2016) 4333–4344.
[24] H.R. Gutiérrez, N. Perea-López, A.L. Elías, A. Berkdemir, B. Wang, R. Lv, F. López-Urías, V.H. Crespi, H. Terrones, M. Terrones, Nano Lett. 13 (2013) 3447–3454.

[25] C. Cong, J. Shang, X. Wu, B. Cao, N. Peimyoo, C. Qiu, L. Sun, T. Yu, Adv. Opt. Mater. 2 (2014) 131–136.
[26] T.V. Shubina, M. Remškar, V.Y. Davydov, K.G. Belyaev, A.A. Toropov, B. Gil, Ann. Phys. 531 (2019), 1800415-1-1800415-14.
[27] Y. Wang, Z. Ma, Y. Chen, M. Zou, M. Yousaf, Y. Yang, L. Yang, A. Cao, R.P.S. Han, Adv. Mater. 28 (2016) 10175–10181.
[28] V. Podzorov, M.E. Gershenson, C. Kloc, R. Zeis, E. Bucher, Appl. Phys. Lett. 84 (2004) 3301–3303.
[29] W. Zhang, Z. Huang, W. Zhang, Y. Li, Nano Res. 7 (2014) 1731–1737.
[30] K. Nassiri Nazif, A. Daus, J. Hong, N. Lee, S. Vaziri, A. Kumar, F. Nitta, M.E. Chen, S. Kananian, R. Islam, K.-H. Kim, J.-H. Park, A.S.Y. Poon, M.L. Brongersma, E. Pop, K.C. Saraswat, Nat. Commun. 12 (2021), 7034-1-7034-9.
[31] C. Zhou, X. Wang, S. Raju, Z. Lin, D. Villaroman, B. Huang, H.L.-W. Chan, M. Chan, Y. Chai, Nanoscale 7 (2015) 8695–8700.
[32] Z. Yu, J. Wang, Phys. Rev. B 91 (2015), 205431-1-205431-10.
[33] G. Ding, Y. Hu, D. Li, X. Wang, D. Qin, J. Adv. Res. 24 (2020) 391–396.
[34] Y. Zhou, J. Dong, H. Li, RSC Adv. 5 (2015) 66852–66860.
[35] X. Yu, H. Dong, L. Wang, Y. Li, RSC Adv. 6 (2016) 80431–80437.
[36] R. Levi, O. Bitton, G. Leitus, R. Tenne, E. Joselevich, Nano Lett. 13 (2013) 3736–3741.
[37] H. Tang, B. Shi, Y. Pan, J. Li, X. Zhang, J. Yan, S. Liu, J. Yang, L. Xu, J. Yang, M. Wu, J. Lu, Adv. Theory Simul. 2 (2019), 1900001-1-1900001-11.
[38] Y. An, M. Zhang, D. Wu, Z. Fu, K. Wang, J. Mater. Chem. C 4 (2016) 10962–10966.
[39] M. Ghorbani-Asl, S. Borini, A. Kuc, T. Heine, Phys. Rev. B 85 (2013), 235434-1-235434-6.
[40] G. Seifert, H. Terrones, M. Terrones, G. Jungnickel, T. Frauenheim, Phys. Rev. Lett. 85 (2000) 146–149.
[41] B.-L. Gao, S.-H. Ke, G. Song, J. Zhang, L. Zhou, G.-N. Li, F. Liang, Y. Wang, C. Dang, J. Alloys Compd. 695 (2017) 2751–2756.
[42] M. Sugahara, H. Kawai, Y. Yomogida, Y. Maniwa, S. Okada, K. Yanagi, Appl. Phys. Express 9 (2016), 75001-1-75001-5.
[43] Y.D. Li, X.L. Li, R.R. He, J. Zhu, Z.X. Deng, J. Am. Chem. Soc. 124 (2002) 1411–1416.
[44] M. Nath, A. Govindaraj, C.N.R. Rao, Adv. Mater. 13 (2001) 283–286.
[45] Y.Q. Zhu, W.K. Hsu, Ni Grobert, B.H. Chang, M. Terrones, H. Terrones, H.W. Kroto, D.R.M. Walton, B.Q. Wei, Chem. Mater. 12 (2000) 1190–1194.
[46] M. Damnjanović, T. Vuković, I. Milošević, Isr. J. Chem. 57 (2017) 450–460.
[47] G. Seifert, H. Terrones, M. Terrones, G. Jungnickel, T. Frauenheim, Solid State Commun. 114 (2000) 245–248.
[48] M. Ghorbani-Asl, N. Zibouche, M. Wahiduzzaman, A.F. Oliveira, A. Kuc, T. Heine, Sci. Rep. 3 (2013) 2961.
[49] A. Grillo, M. Passacantando, A. Zak, A. Pelella, A.D. Bartolomeo, Small 16 (2020), 2002880.
[50] S. Boker, M. Neale, H. Maes, M. Wilde, M. Spiegel, T. Brick, J. Spies, R. Estabrook, S. Kenny, T. Bates, P. Mehta, J. Fox, Psychometrika 76 (2011) 306–317.
[51] H.J. Monkhorst, J.D. Pack, Phys. Rev. B 13 (1976) 5188–5192.
[52] C.G. Broyden, IMA J. Appl. Math. 6 (1) (1970) 76–90.
[53] R. Fletcher, Comput. J. 13 (3) (1970) 317–322.
[54] D. Goldfarb, Math. Comput. 24 (109) (1970) 23–26.
[55] D. F Shanno, Math. Comput. 24 (111) (1970) 647–656.
[56] A. Banerjee, N. Adams, J. Simons, R. Shepard, J. Phys. Chem. 89 (1) (1985) 52–57.
[57] P. Csaszar, P. Pulay, J. Mol. Struct. 114 (1984) 31–34.
[58] J.P. Perdew, Phys. Rev. B 33 (1986) 8822–8824.
[59] M.P. Lopez Sancho, J.M. Lopez Sancho, J. Rubio, J. Phys. F Met. Phys. 14 (1984) 1205–1215.
[60] C. Xie, H. Yuan, Z. Zhang, X. Wang, Phys. Rev. Mat. 6 (2022), 094406-1-094406-8.
[61] J. Wang, H. Yuan, Y. Liu, X. Wang, G. Zhang, Phys. Rev. B 106 (2022). L060407-1-L060407-6.
[62] G. Ding, J. Wang, Z.-M. Yu, Z. Zhang, W. Wang, X. Wang, Phys. Rev. Mat. 7 (2023), 014202-1- 014202-8.
[63] J. Kumar, H.B. Nemade, P.K. Giri, Phys. Chem. Chem. Phys. 19 (2017) 29685–29692.
[64] Y. Zhang, Q. Lv, A. Fan, L. Yu, H. Wang, W. Ma, R. Lv, X. Zhang, Nano Res. 15 (2022) 9578–9587.
[65] L.D. Hicks, M.S. Dresselhaus, Phys. Rev. B 47 (1993), 12727.
[66] J. He, M.G. Kanatzidis, V.P. Dravid, Mater. Today 16 (2013) 166.
[67] T.H. Kim, J. Lee, R.-G. Lee, Y.-H. Kim, npj Comput. Mater. 8 (2022) 1–8.
[68] C. Zhou, M.R. Deshpande, M.A. Reed, L. Jones II, J.M. Tour, Appl. Phys. Lett. 71 (1997) 611–613.
[69] G. Hu, K. He, S. Xie, A. Saxena, J. Chem. Phys. 129 (2008), 234708-1-234708-7.